AIP | The Journal of Chemical Physics

# Energy-scales convergence for optimal and robust quantum transport in photosynthetic complexes

M. Mohseni, A. Shabani, S. Lloyd, and H. Rabitz

Citation: The Journal of Chemical Physics **140**, 035102 (2014); doi: 10.1063/1.4856795
View online: http://dx.doi.org/10.1063/1.4856795
View Table of Contents: http://scitation.aip.org/content/aip/journal/jcp/140/3?ver=pdfcov
Published by the AIP Publishing



# Energy-scales convergence for optimal and robust quantum transport in photosynthetic complexes

M. Mohseni,[1,2] A. Shabani,[3,4] S. Lloyd,[5] and H. Rabitz[3]
[1]*Google Research, Venice, California 90291, USA*
[2]*Research Laboratory of Electronics, Massachusetts Institute of Technology, Cambridge, Massachusetts 02139, USA*
[3]*Department of Chemistry, Princeton University, Princeton, New Jersey 08544, USA*
[4]*Department of Chemistry, University of California at Berkeley, Berkeley, California 94720, USA*
[5]*Department of Mechanical Engineering, Massachusetts Institute of Technology, Cambridge, Massachusetts 02139, USA*

(Received 22 July 2013; accepted 3 December 2013; published online 21 January 2014)

Underlying physical principles for the high efficiency of excitation energy transfer in light-harvesting complexes are not fully understood. Notably, the degree of robustness of these systems for transporting energy is not known considering their realistic interactions with vibrational and radiative environments within the surrounding solvent and scaffold proteins. In this work, we employ an efficient technique to estimate energy transfer efficiency of such complex excitonic systems. We observe that the dynamics of the Fenna-Matthews-Olson (FMO) complex leads to optimal and robust energy transport due to a convergence of energy scales among all important internal and external parameters. In particular, we show that the FMO energy transfer efficiency is optimum and stable with respect to important parameters of environmental interactions including reorganization energy $\lambda$, bath frequency cutoff $\gamma$, temperature $T$, and bath spatial correlations. We identify the ratio of $k_B\lambda T/\hbar\gamma g$ as a single key parameter governing quantum transport efficiency, where g is the average excitonic energy gap.  [http://dx.doi.org/10.1063/1.4856795]

## I. INTRODUCTION

Life on the earth has been solar-powered via the mechanism of photosynthesis for $4 \times 10^9$ years.[1] Photosynthetic antenna complexes have evolved to harvest the sun's energy and efficiently transport it to reaction centers where it is stored as biochemical energy. The first few steps in photosynthesis represent highly sophisticated energy capture and transfer processes, as in an efficient solar cell. Specialized pigments in the antenna complexes absorb energy from sunlight, creating electron-hole pairs known as *excitons*. The excitons then travel to reaction centers where their energy is converted and stored as chemical energy. The key feature for the success of photosynthesis is the high efficiency of exciton transport—as high as 99% in certain bacterial systems.[2] Thus, photosynthetic complexes provide an excellent model for designing efficient artificial excitonic devices. Unfortunately, the fundamental structural and dynamical processes contributing to such efficient migration of excitons are not fully understood. Despite tremendous progress in theory and experiment in the past four decades,[3–47] it is not known how efficient and robust are theses complexes with respect to variations to environmental parameters. In this work, we address this question.

Here, we observe that the Fenna-Matthews-Olson (FMO) pigment-protein complex is optimal and robust with respect to the estimated parameters of the system and environmental interactions. We show that efficient and fault-tolerant energy transport occurs when the FMO internal parameters are in tune with environmental parameters leading to a collaborative interplay of the coherent free Hamiltonian evolution and incoherent effects due to environment. We comprehensively study the effects of reorganization energy $\lambda$, bath frequency cutoff $\gamma$, temperature $T$, positive and negative spatial correlations on the energy transfer efficiency (ETE) landscapes. We show that ETE is optimal for the physiologically estimated value of these parameters, and is robust over a wide range of variations in these parameters. We demonstrate that a convergence of time/energy scales for the relevant internal end environmental parameters of FMO complex facilitates efficient energy transport. For an excitonic system with average energy gap $g$, we observe that a single effective parameter $\Lambda = k_B\lambda T/\hbar\gamma g$ governs the behavior of quantum transport dynamics. Small values $\Lambda \ll 1$ give rise to weak localization and low efficiency. Intermediate values $\Lambda \approx 1$ correspond to the optimal energy transfer. Large values $\Lambda \gg 1$ give rise to strong (dynamical) localization and low efficiency. We also observe that positive/negative spatial correlations essentially renormalize the reorganization energy to effective lower/higher values. The positive bath correlations can significantly enhance ETE at the regime of large $\lambda$ by inducing symmetries in the effective phonon-exciton Hamiltonian protecting the transport against strong dynamical disorder. In the intermediate values of system-bath coupling, the spatial correlations can enhance the robustness of transport efficiency. However, at the very small values of reorganization energy, they have an adversarial effect by diminishing useful but weak

 

bath fluctuations. Overall we conclude that the convergence of timescales effectively acts to increase both efficiency and robustness. Such a mechanism could serve as a key principle for designing novel materials to achieve enhanced quantum transport in dissipative and disorder environments.

Recently there have been a considerable interest in exploring the interplay of the excitonic Hamiltonian with a dissipating environment to explain the efficiency of light harvesting systems.[32–36] In Ref. 32 it was demonstrated that an effective collaboration between coherent quantum evolution and environmental fluctuations could enhance photosynthetic ETE. This work was based on a quantum trajectory picture,[32] within the Born-Markov and secular approximations which guarantee complete positivity of the excitonic dynamics.[48] However, due to the perturbative approximation used in this model, it was impossible to explore the optimality of energy transfer efficiency in the regimes of intermediate system-bath coupling strength. Moreover, due to secular approximation, the coherence and population transfers are essentially decoupled. In order to avoid such problems subsequent studies relied on non-perturbative Haken-Strobl method[9] to be able to explore a wider range of environmental interactions in the context of a (pure-dephasing) classical white-noise model at infinite temperature. These model studies illustrate optimal ranges of dephasing-assisted excitation transfer.[34–36] In the optimal regime, an appropriate level of environmental fluctuations can wash out the quantum localization effects at the equilibrium state, when they are not too strong to lead to quantum Zeno effect.[34] These models, however, are by construction inadequate to capture the role of quantum interplay of system evolution with non-equilibrium dynamics of bath within realistic non-perturbative and non-Markovian regimes.[38]

In principle one can employ a Hierarchy Equation of Motion (HEOM), which was introduced by Kubo and Tanimura,[49] to capture the complete dynamics of quantum systems in the limit of an infinite set of coupled differential equations. However, full HEOM has exponential complexity with the size of the system, the bath correlation time-scale, and within low temperature regimes. Thus in practice HEOMs require severe truncations and they are no longer exact when they applied to a given system.[39] The essential physics behind the hierarchy is that a complex spectral density can be described by a few collective bath coordinates. A systematic derivation of this picture for aggregates was developed in Refs. 4 and 5. The transport equations derived in Zhang *et al.*[5] provide analytical expressions for polaron effects and interpolate between the Redfield and Förster limits. These are much simpler models than the hierarchy and reproduce the same physics.[4–6] Over the past few years, a number of alternative or complementary techniques for simulation of open quantum dynamics have been proposed.[48,50–56] Recently, we have shown that the second-order time-convolution (TC2) master equation can be used to efficiently estimate ETE in large complex excitonic systems interacting with bosonic environments in the *intermediate* regimes.[20] We have also examined the TC2 master equation reliability beyond extreme Markovian and perturbative limits.[20] This is the method that we employ in this work.

The organization of the paper is as follows: Sec. II reviews the TC2 master equation that we employ to efficiently simulate energy transport in multichromophoric systems in low excitation regimes.[20] In Sec. III, the efficiency and sensitivity of the FMO is studied with respect to the environmental parameters including reorganization energy, bath cutoff frequency, temperature, and bath spatial correlations. In Sec. VIII, we argue the possibility of a so-called *Goldilocks principle* in the quantum regime that could explain the convergence of time-scales in FMO complex and other light-harvesting systems. Some complementary materials for FMO complex are presented in Appendices on the FMO structural data and ETE in the presence of an Ohmic bath.

## II. THEORETICAL MODEL

The dynamics of a multichromophoric system interacting with surrounding scaffold protein and solvent can be understood by starting from a general time evolution formulation of open quantum systems. The total system-bath Hamiltonian can be expressed as

$$H_{total} = H_S + H_{ph} + H_{S-ph}, \tag{1}$$

where

$$H_S = \sum_{j,k} \epsilon_j |j\rangle\langle j| + J_{jk}|j\rangle\langle k|,$$

$$H_{ph} = \sum_{j,\xi} \hbar\omega_\xi \left(p_{j,\xi}^2 + q_{j,\xi}^2\right)/2,$$

$$H_{S-ph} = \sum_j S_j B_j.$$

The phonon bath is modeled as a set of harmonic oscillators.[57] Here $|j\rangle$ denotes an excitation state in a chromophore spatially located at site $j$. The diagonal site energies are denoted by $\epsilon_j$s that include reorganization energy shifts $\lambda_j = \sum_\xi \hbar\omega_\xi d_{j,\xi}^2/2$ due to interactions with a phonon bath; $d_{j,\xi}$ is the dimensionless displacement of the $(j, \xi)$th phonon mode from its equilibrium configuration. The strengths of dipole-dipole interactions between chromophores in different sites are represented by $J_{jk}$. The operators $S_i = |j\rangle\langle j|$ and $B_j = -\sum_\xi \hbar\omega_\xi d_{j,\xi} q_{j,\xi}$ are system and bath operators. Here, we assume that each site is linearly interacting with a separate phonon bath. In Ref. 20 we showed that for the range of parameters being considered in this study, we can employ time-nonlocal master equation, e.g., TC2,[20] to describe the decoherence dynamics as modeled above:

$$\frac{\partial}{\partial t}\rho(t) = \mathcal{L}_S\rho(t) + \mathcal{L}_{e-h}\rho(t) - \sum_j \left[S_j, \frac{1}{\hbar^2}\int_0^t C_j(t-t')e^{\mathcal{L}_S(t-t')} \times S_j\rho(t')dt' - h.c.\right], \tag{2}$$

where $C_j(t-t_1) = \langle \tilde{B}_j(t)\tilde{B}_j(t_1)\rangle$ represent the bath correlation function, and the Liouvillian superoperators $\mathcal{L}_S$, $\mathcal{L}_{ph}$, and $\mathcal{L}_{S-ph}$ associated to $H_S$, $H_{ph}$, and $H_{S-ph}$, respectively. The term $\mathcal{L}_{e-h} = -\sum_j r_{loss}^j\{|j\rangle\langle j|, .\} - r_{trap}\{|trap\rangle\langle trap|, .\}$

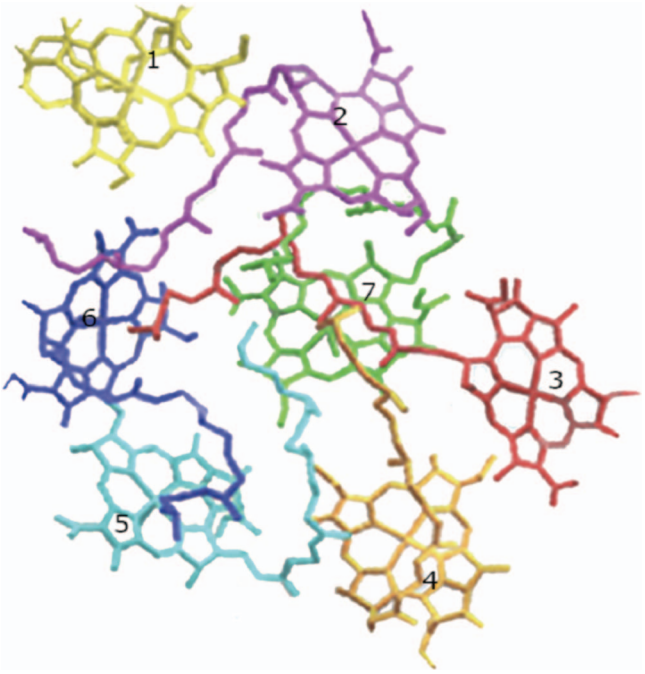


FIG. 1. The disordered structure of the Fenna-Matthews-Olson (FMO) complex. It is a trimer consisting of three identical monomers each formed from seven BChls embedded in a scaffold protein. The FMO complex acts as an energy transfer channel in green sulphur bacteria guiding excitons from the light-harvesting antenna complex, in the proximity of BChls 1 and 6, to the reaction center which is in the proximity of BChls 3 and 4.

captures two different competing electron-hole pair recombination processes that determine the energy transfer efficiency of light harvesting complexes. The first process is the loss due to dissipation to the environment at each site that happens within the time-scale of 1 ns. This inevitable adverse environmental effect guarantees that the energy transfer efficiency has a value less than one. The second process is the desired recombination process due to successful trapping. The ETE is defined as accumulated probability of exciton being successfully trapped:

$$\eta = 2r_{trap}\int_0^\infty \langle trap|\rho(t)|trap\rangle dt. \tag{3}$$

The above performance function is biologically relevant and has been extensively used for a variety of light-harvesting complexes.[12,20,32]

In this work, we concentrate on the dynamics of the FMO pigment-protein complex of the bacterium *Chlorobium tepidum*[62] as a prototype for larger light-harvesting antenna complexes (Fig. 1). The structure of this pigment-protein complex was the first of light-harvesting complexes to be determined by x-ray crystallography.[61] The FMO structure consists of a trimer, formed by three identical monomers, each includes a closely packed assembly of seven BChl-a molecules. The FMO trimer guides excitation energy transfer between the chlorosome, the light-harvesting antennae of green sulfur bacteria, and the membrane-embedded type I reaction center (RC). In Secs. III–V for our numerical simulations, unless specified otherwise, the environmental parameters for the FMO complex are chosen according to the experimentally or theoretically estimated values of reorganization energy

TABLE I. Fixed parameter used in simulations.

| $\lambda$ | $\gamma$ | $T$ | $r_{trap}^{-1}$ | $r_{loss}^{-1}$ |
|---|---|---|---|---|
| 35 $cm^{-1}$ | 50 $cm^{-1}$ | 298 K | 1 ps | 1 ns |

35 $cm^{-1}$, temperature 298 K, trapping rate of 1 ps, exciton life-time of 1 ns, and zero spatial correlations. In the present simulations, we adopt the bath cutoff frequency of 50 $cm^{-1}$ from the studies in Refs. 7 and 71. However, we have repeated our simulations for another reported estimation of $\gamma = 166$ $cm^{-1}$, Ref. 58, and we observed no significant difference in the behavior of ETE landscape. The fixed value of parameters are summarized in Table I.

The diagonal and off-diagonal free Hamiltonian parameters are given in Appendix A, as functions of chromophoric distances, dipole moment angles, and site energies. The trapping rate is treated as a free parameter in Sec. IV. For most of this paper we assume an excitation initially localized at site 1. Similar results are obtained for other initializations such as localized state at site 6. In Sec. III, we use Eq. (3) to demonstrate efficiency and robustness of the FMO complex with respect to variations in reorganization energy, temporal correlations, temperature, and spatial correlations.

We employ the time-nonlocal master equation presented above to efficiently estimate the energy transfer efficiency *landscape* as a function of various environmental degrees of freedom over a wide range of values. This efficient simulation allows us to examine comprehensively all relevant regimes of the multiparameter space for finding possible high efficient and robust neighborhoods. Only after such exhaustive study can one quantify the performance of any particular natural photosynthetic complexes. Moreover, such studies shed light on the maximum capabilities that can be achieved for optimal material design to engineer and characterize fault-tolerant artificial light-harvesting systems[59,60] within a given rich system-environmental parameter space. The quantum efficiency of photosynthetic energy conversion can also be estimated by measuring the quantum requirements of ATP (adenosine triphosphate) formation.[2] Thus, the overall robustness and optimality of a pigment-protein complex can also be experimentally explored, verified, or calibrated by varying the tunable parameters in the laboratory. For example, this can be achieved by changing ambient temperature and using diverse solvents with different dielectric properties.[60]

## III. OPTIMALITY AND ROBUSTNESS WITH RESPECT TO REORGANIZATION ENERGY AND NON-MARKOVIANITY

We first explore the variation of the FMO energy transfer efficiency versus reorganization energy and bath cutoff frequency using a Lorentzian spectral density (see Fig. 2). The reorganization energy, $\lambda$, is proportional to the squared value of the system-bath couplings, quantifying the decoherence strength. The bath cutoff frequency is the inverse of the bath coherence time-scale that captures the non-Markovian nature of the environment. That is, the non-Markovianity measure, defined as the information flow from the system to the phonon bath by Breuer *et al.*[63] increases exponentially with

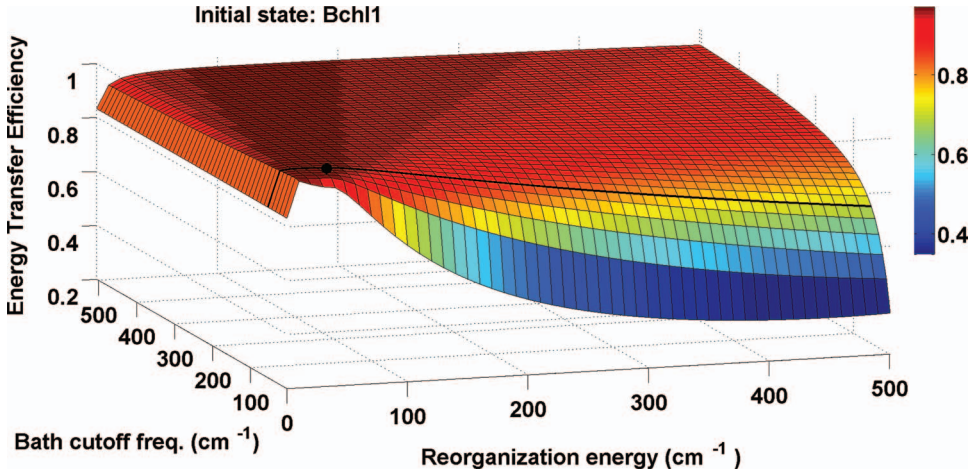


FIG. 2. The energy transfer efficiency (ETE) of the Fenna-Matthews-Olson complex versus reorganization energy $\lambda$ (as a measure of decoherence strength) and bath cutoff frequency $\gamma$ (as a measure of non-Markovian character of the bath[63,64]). The experimentally estimated values of $T = 298$ K, $\lambda = 35$ cm$^{-1}$, $\gamma = 50$–$166$ cm$^{-1}$, $r_{trap}^{-1} = 1$ ps, and $r_{loss}^{-1} = 1$ ns reside at an optimal and robust neighborhood of ETE. The FMO complex would act sub-optimally in the regimes of large $\gamma$ and very small $\lambda$, or large $\lambda$ and very small $\gamma$. In the intermediate values of $\lambda/\gamma$ the phenomenon of environment-assisted quantum transport takes place. A top view of this plot in Fig. 3 indicates $\lambda/\gamma$ is the parameter that governs efficiency at a fixed temperature.

decreasing bath cutoff frequency.[64] The ETE function has not been illustrated in Fig. 2 for bath cutoff frequency values less than $\gamma = 5$ cm$^{-1}$ , since according to our analysis in Ref. 20 the simulation errors of TC2 master equation may become significant in such highly non-Markovian regimes. It should be noted that in the regime of $\hbar\gamma > k_B T$ we apply low temperature corrections to the bath correlation function as explained in Sec. IV. The optimality and robustness of ETE for the FMO protein complex at the experimentally estimated values of $\lambda = 35$ cm$^{-1}$ and $\gamma = 50$–$166$ cm$^{-1}$ are evident in Fig. 2. An independent study on the optimality of ETE versus reorganization energy has been reported in Ref. 65. It can be observed in Fig. 2 that the non-Markovianity of the bath can slightly increase ETE in the regimes of weak system-bath coupling. However, such slow bath behavior can significantly decrease ETE when the system interacts strongly with it. The main question is how one can understand this phenomenon for all non-Markovian and Markovian regimes in the context of Environment-Assisted Quantum Transport (ENAQT), which was first investigated using simplified formalisms of the Lindblad (weak coupling and Markovian assumptions)[32] and Haken-Strobl (infinite temperature, pure-dephasing assumption).[33]

In this work, we report an underlying theory for environment-assisted quantum transport. The landscape in Fig. 2 shows a remarkable interplay of reorganization energies $\lambda$ and bath frequency cutoff $\gamma$. The ETE takes values below unity if the FMO operates at the limit of very small $\lambda$ and large $\gamma$. On the other limit, the FMO efficiency drops significantly when operating at large $\lambda$ and very small $\gamma$. As we argue below these two regimes can be understood as manifestations of weak- and strong quantum localization, respectively.

A note on terminology: we use the terms weak and strong localization in analogue to the corresponding effects in bulk solid-state systems.[67] However, in contrast to solid state systems, here we are dealing with finite-size systems of few chromophores. In addition, it is important to note that because of the long-range nature of the dipolar force, the bulk versions of these chromophoric systems would not exhibit exponentially localized states. What is really being investigated here, then is a kind of *transient* localization which would eventually go away due to the long-range nature of the dipolar force and the small system size. If the destruction of transient localization takes longer than the exciton lifetime, however, then transient localization is just as adversarial to quantum transport efficiency as full localization. In this paper, when we refer to weak and strong localization, the reader should keep in mind that we are actually discussing weak and strong transient localization.

In order to fully explore the regimes of weak and strong localization and the various intermediate transitional regions, we illustrate a top view of Fig. 2 in Fig. 3. This plot

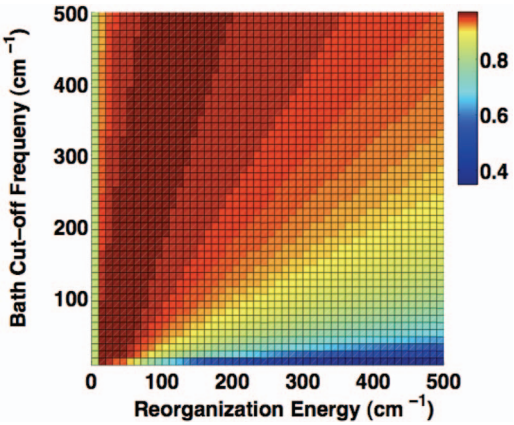


FIG. 3. Top view of ETE landscape illustrated in Fig. 2 indicating that the ratio of the reorganization energy over bath frequency cutoff can be considered as the parameter that governs the energy transfer efficiency at a fixed temperature. As we inspect this plot in an angular coordinate from the vertical axis, $\gamma$, toward the horizontal axis, $\lambda$, we can distinguish different regions of the ETE landscape that are separated by straight lines $\lambda/\gamma$. At very small decoherence rate, the FMO complex experiences weak localization due to static disorder. As we increase this ratio, an optimal region of ETE emerges that is induced by an appropriate level of interplay between environmental fluctuations and coherent evolution. At higher levels of this parameter, ETE drops significantly due to strong localization induced by dynamical disorder.

immediately reveals that the regions of distinct energy transfer efficiencies at room temperature are governed by a parameter of the form $\lambda/\gamma$. For small and for large values of this parameter, the efficiency is low. The efficiency reaches its maximum for intermediate values of this parameter. In both strong and weak quantum localization limits the excitation will be spatially trapped in the regions typically far from reaction center and eventually dissipating to bath due to adversarial electron-hole recombination processes which occur on three orders of magnitude slower time-scale. In the intermediate regime, the right amount of the interplay of quantum coherence and environmental fluctuations can facilitate an optimal energy transport in a robust fashion by various physical mechanisms including minimizing site energy mismatches, washing out potential destructive quantum interference effects, and enhancing the energy funneling by providing an appropriate vibrational energy sink.

The dependence of efficiency on $\lambda/\gamma$ can be understood as follows. When the FMO complex interacts weakly with its environment the exciton migration is essentially dictated by the site energies and inter-pigment couplings. The spatial locations, Fig. 1, and dipole moments of BChls do not show any obvious regular pattern. In the absence of environmental interactions, destructive interference effects due to such random configurations can cause weak localization over a few chromophores away from the trapping site. This phenomenon prevents successful delivery of the initial exciton to the reaction center and therefore leads to below unity efficiency of about 83% at $\lambda = 0$. Weak localization is amplified by lowering the temperature, a behavior observed in the simulations presented in Sec. IV. By increasing the system-bath coupling strength, the adversarial interference effects of excitonic pathways are diminished in a fashion similar to observations reported in Refs. 32, 33, and 35. However, here it can be observed in Fig. 3 that for larger bath cutoff frequencies, a larger reorganization energy is required for ENAQT to occur.

We can understand these observations in terms of ENAQT by noting that the effective decoherence rate is given by $\lambda/\gamma$ in the perturbative limit at a fixed temperature.[48] This ratio becomes smaller as we raise the $\gamma$ therefore a stronger coupling $\lambda$ is needed to guarantee the level of decoherence strength required for ENAQT. The overlap of a delocalized exciton wave function with the trap enables an almost complete, 98% quantum transport in the optimal range of $\lambda/\gamma$ at the ambient temperature. As we increase the reorganization energy and bath coherence time-scale, the ETE starts to drop. In this regime, excitonic wave function again experiences localization as the environmental fluctuations change their role to play a strong adversarial effect on the quantum transport essentially as a source of strong dynamical disorder. The ETE landscape in Fig. 3, clearly has level sets that exhibit linear relationship with $\lambda$ and $\gamma$. Indeed the ratio $\lambda/\gamma$, known as the Kubo number, is the parameter that governs Anderson localization transition in stochastic classical modeling of environmental interactions.[67–70] In the fixed high-temperature limit of ETE illustrated in Fig. 3, one can observe that $\lambda/\gamma$ is a determining parameter for transport efficiency in the regions beyond optimal ENAQT area. In Sec. IV, we go beyond the Kubo number, by directly investigating the temperature dependent energy transfer dynamics, leading to a general governing parameter as $k_B\lambda T/\hbar\gamma$.

The theoretical and experimental modeling of the environment surrounding the FMO complex suggests that the spectral density of the phonon bath modes can be expressed as a sum of a few Lorentzian terms.[57] The spectral density function $J(\omega)$ determines the time correlation functions as

$$\langle \tilde{B}(t)\tilde{B}(0)\rangle = \frac{1}{\pi}\int_0^\infty d\omega J(\omega)\frac{\exp(-i\omega t)}{1-\exp(-\hbar\omega/k_BT)}, \quad (4)$$

where a Lorentzian spectral function has the form $J(\omega) = 2\lambda\omega/(\omega^2+\gamma^2)$. For simplicity in this work we have considered a single Lorentzian term with amplitude $\lambda = 35\ \mathrm{cm}^{-1}$ and cutoff frequency $\gamma = 50\ \mathrm{cm}^{-1}$. However, these values were actually extracted by fitting the experimentally measured absorption spectrum using an Ohmic spectral density $J(\omega) = \lambda(\omega/\gamma)\exp(-\omega/\gamma)$.[71] Thus, we also examine ETE versus variations of $\lambda$ and $\gamma$ in such a model depicted in Fig. 8, see Appendix B. We note that for an Ohmic model a very similar behavior of the optimality and robustness of energy transport can be observed as those in Fig. 2; however, the estimated ETE is lower than those obtained by exploiting a Lorentzian model. Specifically for FMO the ETE values are 92.3% and 96.7% for Ohmic and Lorentzian spectral density, respectively. This suggests that an Ohmic bath cannot capture the near unity efficiency of FMO complex, and favors the Lorentzian model as a more accurate description of the bath spectral density.

## IV. OPTIMALITY AND ROBUSTNESS WITH RESPECT TO REORGANIZATION ENERGY AND TEMPERATURE

Here, we directly examine the temperature dependence of the effective parameter $\lambda/\gamma$ discussed in Sec. III. Generally light-harvesting complexes in bacterial, marine algae, and higher plants operate at various temperatures and reorganization energies. For example, the FMO complex of the green sulfur bacteria can operate at the bottom of the ocean at a depth of hundreds of meters, and also in hot springs with diverse temperature variations. Moreover, 2D electronic spectroscopy of these systems has been performed at different cryogenic and room temperatures. Thus, we need to explore the efficiency and sensitivity of energy transport as a function of reorganization energy and temperature.

We note that in the low temperature limit, $\hbar\gamma > k_BT$, the Lorentzian bath correlation function $\langle \tilde{B}(t)\tilde{B}(t')\rangle_{ph}$ is no longer a single term $\lambda(2k_BT/\hbar - i\gamma)e^{-\gamma(t-t')}$ and should be corrected by a sum of exponentially decaying terms

$$\langle \tilde{B}(t)\tilde{B}(t')\rangle_{ph} = \frac{\gamma\lambda}{\hbar}\left(\cot\left(\frac{\hbar\gamma}{2k_BT}\right) - i\right)e^{-\gamma(t-t')} + \frac{4\lambda\gamma k_BT}{\hbar^2}\sum_{k=1}^{\infty}\frac{\nu_k}{\nu_k^2-\gamma^2}e^{-\nu_k(t-t')}, \quad (5)$$

where $\nu_k = 2\pi k(k_BT)\hbar$ are bosonic Matsubara frequencies. In practice a truncation of the above infinite series is needed for numerical simulations. The higher levels of truncation are dictated by lower temperature limits for the systems under study. To guarantee an accurate estimation of the bath

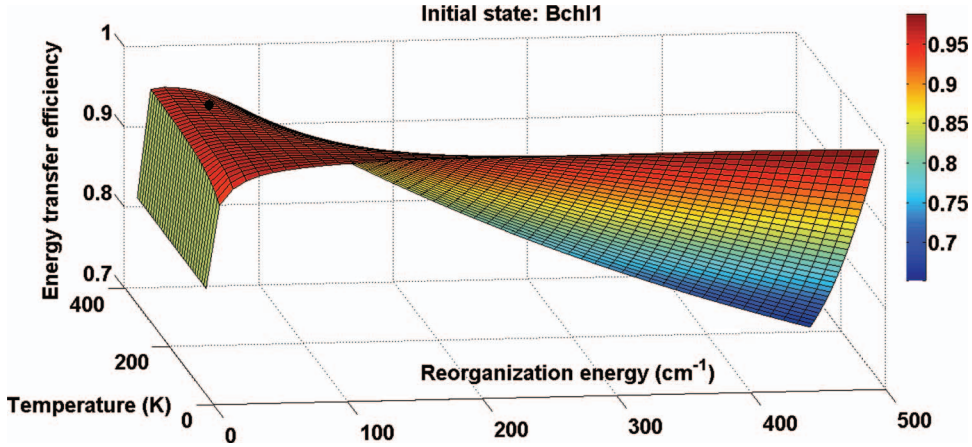


FIG. 4. Energy transfer efficiency manifold as a function of reorganization energy and temperature. The temperature range is from 35 K to 350 K. At the regimes of large system-bath coupling strength the ETE drops faster by increasing the temperature due to strong localization induced by dynamical disorder. There is a narrow region of reorganization energies between 10 and 50 $cm^{-1}$ that ETE is relatively robust with respect to variations in temperature. The FMO value of $\lambda = 35$ $cm^{-1}$ is located in this region indicating a significant insensitivity to temperature variations. At very low reorganization energy and low temperatures weak localization can be observed due to static disorder.

correlation function for the calculation of energy transfer landscape, in the relevant low temperatures, we consider the first 100 Matsubara frequencies in the above summation. It should be noted that the mentioned low temperature corrections have a minor numerical cost for calculating ETE by using TC2 (2), since we just need to compute sum of the Laplace transforms of the above exponential terms.[20] This is another advantage of using the TC2 in contrast to the more accurate approaches such as HEOM for which every correction term $\nu_k e^{-\nu_k(t-t')}$ necessitates considering $N$ extra auxiliary variables in the simulation, where $N$ is the number of the sites, therefore significantly increasing the computational cost of the simulations.

We show the behavior of ETE as a function of reorganization energy $\lambda$ and temperature $T$ in Fig. 4. It can be observed that at various possible conditions for the FMO protein of $T = 280$ to 350 K and $\lambda = 35$ $cm^{-1}$, the ETE has an optimal value and resides in a robust region of the energy transfer landscape. We note that for system-bath strength corresponding to the FMO's environment, the energy transport is very robust to variations of temperature and just slightly decreases in the low temperature limit. By increasing the reorganization energy, the temperature dependence of ETE becomes more pronounced. As we move toward the classical regime of the dynamics at high reorganization energy and high temperature ETE drops significantly. This implies the necessity of quantum effects for highly efficient and robust excitonic energy transfer. It is remarkable that at the relevant physiological temperatures, the ETE is robust only within the range of $\lambda = 35$ $cm^{-1}$, and it becomes unstable as we approach reorganization energy of over 100 $cm^{-1}$. On the other hand, at the very low temperatures, enhancement of $\lambda$ would improve the ETE and brings it to a saturated high level.

As shown in Sec. III, the parameter $\lambda/\gamma$ governs the shape of the ETE landscape at a fixed high-temperature limit. However, in the perturbative limit the decoherence rate can be expressed by $k_B\lambda T/\hbar\gamma$ which captures the suboptimal ETE in the weak localization region. Now, we investigate if the ETE behavior in all regimes can be globally captured by the parameter $k_B\lambda T/\hbar\gamma$, for the given FMO Hamiltonian. Specifically, we need to verify if one can predict the optimal noise-assisted transport region as well as ETE suppression levels at the strong localization regions by a single parameter $k_B\lambda T/\hbar\gamma$. To examine the validity of this theory, we study ETE as a function of the reorganization energy and the inverse temperature for the fixed $\gamma = 50$ $cm^{-1}$ (see Fig. 5). Similar to the plot of efficiency as a function of $\lambda$, $\gamma$, Fig. 3, here also the efficiency landscape is divided by lines of approximately $k_B\lambda T/\hbar$ (with some deviations from linearity in the high $\lambda$ and low temperature regime). It can be observed from the Fig. 5 that for small $k_B\lambda T/\hbar$ weak localization is dominant. At the intermediate $k_B\lambda T/\hbar$ values environment-assisted energy transport occurs. As we move towards larger system-bath interactions and higher temperatures, strong dynamical disorder diminishes the coherence and the exciton migration can be fully described by an incoherent hopping process, since the wave function is essentially localized over

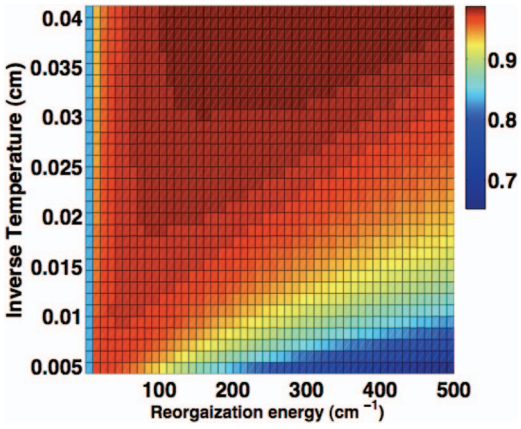


FIG. 5. The top view of the ETE landscape presented in Fig. 4 as a function of inverse temperature and reorganization energy. In the high temperature regime ($k_BT > \hbar\gamma$), the three regions of weak localization, ENAQT and strong localization can be distinguished by the parameter $k_B\lambda T/\hbar$ given the free Hamiltonian of FMO and $\gamma = 50$ $cm^{-1}$. These results, combined with Fig. 3 suggest that the parameter $k_B\lambda T/\hbar\gamma$ governs the shape of the overall FMO energy transfer landscape.

spatial sites. At this regime, the effect of high temperature can be understood from the dynamics of BChls energy fluctuations which is described by the symmetrized correlation function $S(t) = \frac{1}{2}\langle\{\tilde{B}(t), \tilde{B}(0)\}\rangle_{ph}$ ($B_j = B$, for any BChl $j$). The function can be extracted experimentally by three-pulse photon echo peak shift measurement. For a Lorentzian density, $S(t) = 2\hbar k_B \lambda T e^{-\gamma t}$, and fixed $\gamma$, the temperature and the reorganization energy determines the amplitude of the site energy fluctuations. Our simulation in Fig. 4 demonstrates that a high efficient energy transfer can be achieved at a *moderate* site energy fluctuations away from both weak and strong localization limits.

Combining different regimes of three important environmental parameters, $\lambda$, $\gamma$, and $T$, the effective decoherence strength $k_B\lambda T/\hbar\gamma$ emerges as the parameter that governs the energy transfer efficiency landscape. For the FMO free Hamiltonian energy gaps, by increasing the single parameter $k_B\lambda T/\hbar\gamma$ from small to intermediate, and from intermediate to large values, one can describe the transition from weak localization to ENAQT, and from ENAQT to strong localization. More generally, when the effective decoherence rate $k_B\lambda T/\hbar\gamma$ is either much smaller or much larger than the typical energy splitting $g$ between delocalized energy eigenstates, then transport is suppressed. Thus, in order to predict the general patterns of quantum transport in generic light-harvesting systems, we should compare the relative strength of $k_B\lambda T/\hbar\gamma$ (with dimension of energy) to the average excitonic energy gap of the free Hamiltonian that can be quantified as $g = \frac{1}{N-1}||H - Tr(H)\mathbb{I}/N||_*$ for an $N$ level system, where the nuclear norm $||X||_*$ is defined as the summation of $X$'s singular values. This follows from the fact that the ETE of a system with a rescaled Hamiltonian $\alpha H$ equals the ETE of a system with Hamiltonian $H$ for which other environmental energy/time scales are renormalized by a factor $1/\alpha$. Here we give a simple proof for this fact.

The efficiency defined in Eq. (3) can be simply calculated as $\eta = 2r_{trap}\langle trap|\tilde{\rho}(s=0)|trap\rangle$ where $\sim$ denotes the Laplace transform. The operator $\tilde{\rho}(s=0)$ can be found by transforming the dynamical equation (2):

$$-\rho(0) = \mathcal{L}_S\tilde{\rho}(0) + \mathcal{L}_{e-h}\tilde{\rho}(0) - \sum_j \left[S_j, \frac{1}{\hbar^2}\tilde{C}(-\mathcal{L}_S)S_j\tilde{\rho}(0) - h.c.\right]. \quad (6)$$

This yields the ETE

$$\eta = -2r_{trap}\langle trap|\mathcal{K}\rho(0)|trap\rangle, \quad (7)$$

where

$$\mathcal{K} = \left(\mathcal{L}_S + \mathcal{L}_{e-h} - \sum_j \left[S_j, \frac{1}{\hbar^2}\tilde{C}(-\mathcal{L}_S)S_j - h.c.\right]\right)^{-1}. \quad (8)$$

The Laplace transform of the correlation function (5) can be found as $\tilde{C}(-\mathcal{L}_S) = \frac{\gamma\lambda}{\hbar(\gamma-\mathcal{L}_S)}(\cot(\frac{\hbar\gamma}{2k_BT}) - i) + \frac{4k_B\lambda\gamma T}{\hbar^2}\sum_{k=1}^{\infty}\frac{\nu_k}{(\nu_k^2-\gamma^2)(\nu_k-\mathcal{L}_S)}$. Considering these explicit expressions, it is easy to see that the system-bath parameters $\{\alpha H, \lambda, \gamma, T, r_{trap}, r_{loss}\}$ yield the same ETE (7) as the parameter set $\{H, \lambda/\alpha, \gamma/\alpha, T/\alpha, r_{trap}/\alpha, r_{loss}/\alpha\}$. We should mention that similar results can be obtained for the hierarchy equation of motion.

Overall, we introduce the dimensionless parameter as $\Lambda = k_B\lambda T/\hbar\gamma g$, as the parameter that governs the energy transfer efficiency landscape. When we approach $\Lambda \approx 1$, the decoherence rate is tuned to give the maximum transport rate. For $\Lambda \ll 1$ and $\Lambda \gg 1$ we move toward weak and strong-type of transient localizations, respectively. To examine the temperature and also spectral density independency of the observed patterns in Figs. 3 and 5, we present the landscape top view of ETE for (a) Lorentzian density at 77K and (b) Ohmic density at 298K, in Appendix B. In both cases a similar pattern can be observed.

In Ref. 66, we explore the interplay of reorganization energy with a variety of Frenkel-exciton free Hamiltonians for systems consist of up to 20 chromophores with modest site energetic disorders. Our numerical studies suggested that in the optimal transport regime the relevant energy scale of the free Hamiltonian, $g$, can be essentially expressed as the average dipole-dipole interactions strength that is $|\mu|^2 n$, where $|\mu|^2$ is the average dipole-moment strength and $n = \frac{8N}{D^3}$ is the density of $N$ chromophores homogenously embedded in a system with size $D$. We will address the significance of the convergence of energy scales in the broader context of complex quantum systems in Sec. VIII.

## V. OPTIMALITY AND ROBUSTNESS WITH RESPECT TO REORGANIZATION ENERGY AND BATH SPATIAL CORRELATIONS

Recently there have been significant interest on the potential role of bath spatial correlations as the underlying physical principle leading to the experimental observations of long-lived quantum coherence in biomolecular systems.[19,24–31,37,40] These correlations have also been the center of attention and debate in the recent theoretical studies of quantum effects in photosynthetic complexes[33,72–74] as a potential positive feature of environmental interactions. The basic intuition is that if the environmental fluctuations are correlated in space, e.g., in the site basis, then they will lead to fairly global quantum phase modulations in exciton basis, similar in spirit to *decoherence-free subspaces* that are studied in detail in quantum information science.[77] Indeed, as demonstrated earlier in Ref. 33, using a Lindblad master equation, positive spatial correlation can enhance the underlying contributions of quantum coherence to ETE according to two different measures based on Green's function methods. However, the overall ETE remains relatively unchanged for the FMO estimated values, as the contribution of relaxation to ETE drops with a similar rate Ref. 33. Here, we are interested in the potential role of quantum correlations in optimality and/or robustness of energy transport rather than enhancing the time-scale of quantum coherence beating.

The TC2 can be generalized to include the effect of both spatial and temporal correlations between protein environments:

$$\frac{\partial}{\partial t}\rho(t) = \mathcal{L}_S\rho(t) + \mathcal{L}_{e-h}\rho(t) - \sum_{j,k}\left[S^j, \frac{1}{\hbar^2}\int_0^t C_{j,k}(t-t')e^{\mathcal{L}_S(t-t')} \times S^k\rho(t')dt' - h.c.\right]. \quad (9)$$

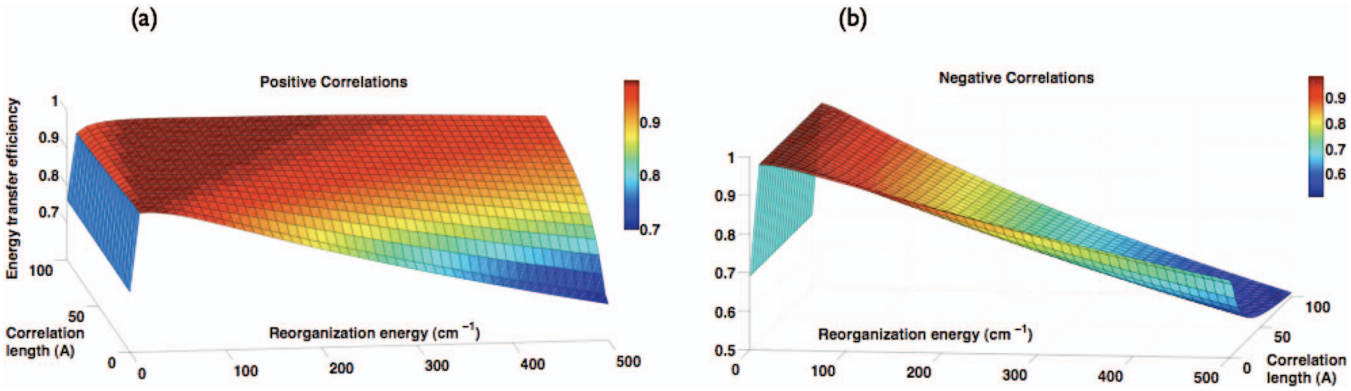


FIG. 6. (a) ETE as a function of reorganization energy and positive bath spatial correlations that correspond to in-phase fluctuations of two spatially separate bath oscillators. At the large values of reorganization energy, the positive correlations induce certain symmetries in the effective phonon-exciton Hamiltonian significantly enhancing ETE, by protecting the system against strong dynamical disorder similar to decoherence free subspaces.[77] In the intermediate values of λ, the ENAQT becomes more robust due to spatial correlations. In large correlation length, the optimal ETE is essentially expanded over a much wider regime, one order of magnitude larger than the optimal ETE region in the absence of any spatial correlations. At smaller values of λ positive spatial correlations actually hinder the exciton transport by decoupling useful but very weak fluctuations. A similar linear relationship is observed here between λ and positive spatial correlations as those with $\gamma$ and $T$. (b) ETE as a function of reorganization energy and negative spatial correlations that correspond to out of phase fluctuations of two spatially separate bath oscillators. Negative correlations reduce ETE at all values of λ.

The function $C_{j,j}$ is just the autocorrelation function of the $j$th environment. The cross correlation between fluctuations of sites $j$ and $k$ is given by the function $C_{j,k}(t-t') = \langle \tilde{B}_j(t)\tilde{B}_k(t')\rangle$. In our study we assume $C_{j,k}$ to be of Lorentzian $\lambda_{j,k}\gamma\omega/(\gamma^2+\omega^2)$ form with the cut-off frequency $\gamma$, similar to the autocorrelation spectral density, and the strength $\lambda_{j,k}$ that decays exponentially with the distance between Bchls $j$ and $k$, $d_{j,k}$. A correlation length $R_{cor}$ determines the strength of the spatial correlations, $\lambda_{j,k} = \lambda\exp(-d_{j,k}/R_{cor})$. We distinguish between the two different cases of positive and negative correlations, corresponding to $\lambda > 0$ and $\lambda < 0$, respectively. The sign of the correlations is imposed by the position and orientation of the Bchls with respect to their surrounding protein.[75]

The effects of positive and negative spatial correlations on the energy transfer efficiency for various degrees of the system-bath couplings are presented in Fig. 6. One main observation is that both positive or negative spatial correlated environmental fluctuations play an insignificant role in the overall ETE only at the regions of reorganization energy very close to $\lambda = 35\,\mathrm{cm}^{-1}$. However, as we slightly increase the system-bath coupling strength, we see two very distinct behaviors of the ETE as a function of long-range spatial characteristics of the bath fluctuations, depending on whether these variations being correlated or anti-correlated. For rather strong reorganization energy, positive spatial correlations can enhance the ETE by about 30%. By contrast, negative spatial correlation can reduce the ETE by the same amount for reorganization energy of above $\lambda = 400\,\mathrm{cm}^{-1}$.

A careful inspection of Fig. 6(a) shows a linear relationship between reorganization energy and positive spatial correlations similar to those with $\gamma$ and $T$, as discussed in Sec. IV. For very small reorganization energies, when quantum localization due to static disorders is present, the positive spatial correlations can slightly reduce ETE by decoupling the fragile but positive role of environmental fluctuations. On the other extreme regime, positive spatial correlations can play a significant positive role by inducing an effective *symmetry* in the system-bath interactions, leading to partial immunity with respect to the strong dynamical disorders at large reorganization energies. Remarkably, in the intermediate regime, the induced symmetries can substantially enhance the robustness of the environment-assisted transport. We can observe that the width of ENAQT region (in reorganization energy axes) is enhanced from $20\,\mathrm{cm}^{-1}$ for zero correlation length to $200\,\mathrm{cm}^{-1}$ for 100 Å correlation length. At this wide regimes, the system is protected with respect to the adversarial effects of dynamical disorder preventing the strong localization effects. Therefore, the spatial correlations should be also incorporated in the governing parameter $k_B\lambda T/\hbar\gamma$. This can be achieved by renormalizing the reorganization energy λ to an effective lower/higher values, when positive/negative correlations exist.

In order to quantify the role of spatial correlations in enhancing the quantum coherence time-scale of light-harvesting complexes, one has to partition the time-nonlocal master equation, Eq. (2), similar in spirit to those studies in Refs. 33 and 41. In Secs. VII and VIII of this work we assume spatial correlations to be negligible for the FMO complex consistent with the recent simulations in Ref. 76. Indeed, the atomistic simulation of the FMO pigment-protein-solvent dynamics at room temperature presented in Ref. 76 reveals insignificant correlations in the site energy fluctuations, suggesting that the uncorrelated bath approximations are reasonably valid.[3,42–47]

## VI. CONVERGENCE OF TIME-SCALES FOR FMO

We illustrate a summary of our main results on the FMO complex energy transport dynamics in the non-Markovian and non-perturbative regimes in Fig. 7. This figure indicates that an effective convergence of time-scales for various dynamical processes exists at the intermediate and optimal regimes (denoted by a white circle) in the energy transfer landscape rep-

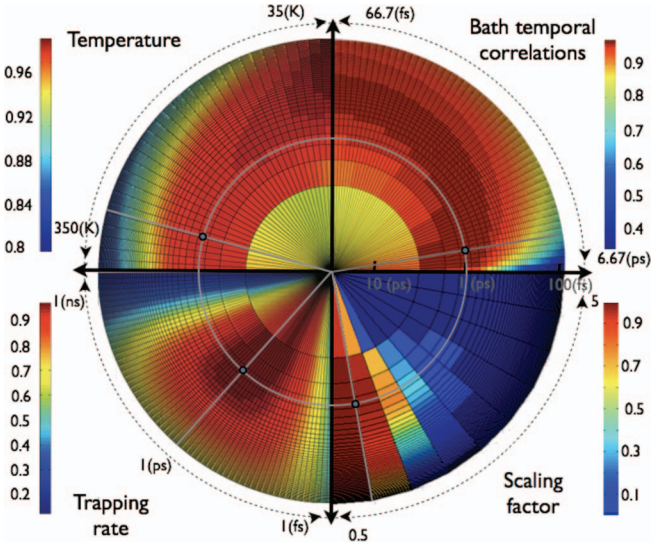


FIG. 7. A summary of our main results on the optimality and robustness of FMO energy transfer dynamics illustrating a convergence of time scale around 1 ps. The radial axes indicate the reorganization energy in logarithmic scale which is essentially the main environmental parameter quantifying the strength of system-bath interactions. Angular coordinate in each quarter represents a different physical quantity. The first three quarters are associated to three other important environmental parameters including bath correlation time-scale, temperature, and trapping time-scale. The last region highlights the role of compactness as the most significant internal parameter of FMO structure quantified by a rescaling factor in the chromophoric relative distances. To improve the clarity the color bar is rescaled in each quarter. The estimated values of the FMO complex coincide in the intermediate values of both angular and radial coordinates, denoted by white lines (around 1 ps), leading to optimal and robust ETE.

resented by a circular surface. The radius of this circular area illustrates the reorganization energy in logarithmic scale in the unit of time from 33.3 ps (1 $cm^{-1}$) to 66.7fs (500 $cm^{-1}$). The circular area consists of four different regions in four quarters, the angular degrees of freedom in each quarter is associated to a different physical quantity. The first quarter represents the degree of the memory in the bath or the non-Markovianity of the environment in logarithmic scale, that is equivalent to bath correlation time, varying from about 6.67 ps to 66.7 fs. The second quarter illustrates variations in the bath temperature from 35 to 350 K. The third region shows six orders of magnitude trapping time-scales from 1 ns to 1 ps in a logarithmic scale. The last quarter demonstrates compactness level of the Frenkel exciton Hamiltonian of the FMO rescaled by a factor from 0.5 to 5. The estimated parameter of the FMO is denoted by a white bar in each region. In all quarters the efficient neighborhood of ETE are somewhere in the medium range, denoted by a white circle at about 1 ps time-scale corresponds to reorganization energy of the FMO. The optimal areas are far from extreme low and high reorganization energies in the center and perimeter of the black circle, respectively, where quantum localization effects can substantially suppress ETE. The key point of this figure is that all the relevant useful transport time-scales converge just around 1 ps, far from the dissipation time-scale of 1 ns. We will discuss the implications of these results in a broader context of optimality and robustness of complex quantum systems in Sec. VIII.

## VII. CONCLUSION

In this work, we studied the structural and dynamical design principles of excitonic energy transfer in the Fenna-Mattews-Olson (FMO) complex. Our numerical simulations demonstrate that the natural structure of FMO pigment-protein complex leads to a highly efficient and robust photosynthetic energy transfer wire. We characterized the ETE landscape by three main regions: weal localization, environment-assisted quantum transport, and strong localization, and identified the scalar $\Lambda = \frac{k_B \lambda T}{\hbar \gamma g}$ as the key parameter to cross between these regions as one hikes over the landscape.

We showed optimality and robustness of energy transport efficiency in FMO with respect to variations in all the main external parameters dictating the dynamics. In particular, we explored the protein-solvent environment factors: system-bath coupling strength, bath memory, temperature, and spatial correlations. We report the robustness with respect to the effects of dissipation, light-harvesting antenna factor: electronic state initialization; reaction center factors; and exciton trapping rate and location in Ref. 85. In that work, we also investigate the performance and sensitivity of the FMO with small and large variations in its internal parameters: chromophoric spatial locations, dipole moment orientations, site energies, and chromophoric density. The exciton trapping process in FMO complex shows to be significantly robust with respect to perturbations in dipole moment orientations and site energies due to its compact structure.[85]

We would like to mention that our study does not necessarily indicate any strong *constructive* quantum dynamical interference to enhance ETE. Those constructive interference effects even if existed will mostly likely not be robust to decoherence. The dynamical role of observed quantum coherence in exciton basis to ETE and their physical (electronic or vibronic) origin still remains open questions, despite recent advances.[78] Those coherence oscillations could be the side effects of the required convergence of coherence and decoherence to achieve robustness and in themselves do not necessarily play any fundamental quantum speed up. However, our numerical study shows that sufficient quantum coherence (due to rather strong coherent dipole-dipole coupling) at least can act as new control knobs for robust engineering of quantum transport in novel material and devices to exploit not-trivial quantum mechanical effects due to non-commuting nature of system Hamiltonian with the system-bath Hamiltonians. These control knobs are mostly ignored as a perturbative effect in the Förster model of excitation energy transfer. We believe that a key design principle for achieving optimal and robust quantum transport performance is to allow for the convergence of energy/time scale of the contributing internal and external parameters. This phenomenon can be regarded as an example of a Goldilocks principle in the quantum regime which we discuss next.

## VIII. DISCUSSION AND OUTLOOK

Our numerical study demonstrated optimality and robustness of FMO with respect to a variety of internal and external

parameters. For FMO, in all cases, we found that the estimated operating values sit nearly at the optimal point for energy transport efficiency, and that there is a relatively wide range of parameters about that point for which FMO is close to optimal. Moreover, we noted that the estimated time/energy scales associated with this point – couplings between sites, reorganization energies, decoherence times, environmental correlation time, and trapping time-scale – all lie in the same intermediate range, of the order of a picosecond. Nevertheless it is instrumental for the FMO performance that life-time of exciton has a sufficiently longer time-scale. For alternative configurations, beyond the specific FMO model, we observed that their chromophoric density, geometrical arrangements, and coupling strengths need to be in tune with environmental interactions to lead to optimal performance.[66] Here, we briefly discuss a possible design principle that fundamentally relies on this convergence of time scales.

A common design technique in engineering is to keep the desired system as simple as possible. The rationale is that overly complex designs are typically not robust: the more complex the design, the harder it is to predict its behavior, and the more pieces there are to fail. Now, FMO and other photosynthetic complexes are definitely not simple: they consist of multiple parts, and, as our studies show, enlist a wide variety of quantum effects, tuning those effects to attain efficient and robust operation. Apparently, these complexes do not obey the fundamental engineering philosophy of *keep it simple*. There is, however, a more sophisticated version of the design principle in system engineering, as overly simple designs may be robust, but they typically also fail to attain their desired functionality. This advanced version of the design principle declares that to the extent that it is possible to add more features to a design to enhance functionality without reducing robustness, it is desirable to do so. That is, given available technologies, there is typically a design that attains a level of complexity that is "just right"—not so simple that it fails to attain its goal, but not so complex that it loses robustnesses. The design strategy that aims for the just-right level of complexity is sometimes called the *Goldilocks principle* for complex systems.[79] Goldilocks principle applies across various areas, particularly the well known concept of Goldilocks or habitable zone in astronomy,[80] efficient search algorithms,[81] nanotechnology,[82] and cell biology.[83]

Here we propose the possibility of a Goldilocks principle in the quantum regime – the *quantum* Goldilocks principle – as a potentially new design principal for complex quantum systems. The quantum Goldilocks principle in this context could state that to improve efficiency, or any other ultrafast performance measure of a complex nanostructure, quantum effects could be used as long as by doing so it does not make the operation of the system more fragile. Our simulations show that this is the case with FMO: a wide variety of parameters have been tuned to their optimal value, and that optimal value is robust against variations in those parameters. The quantum Goldilocks principle essentially explains why it is beneficial for certain parameters that involve time or energy to converge to the same time/energy scale.

When the time scale for one effect is very different from the time scale for another, then the first effect can typically be regarded as a perturbation on the other. For example, if the environmental interactions are much slower than the system internal dynamics, and/or if the correlation time of the environment is much shorter than the coherent tunneling rate of an exciton from chromophore to chromophore, then the effect of the environment can be treated in the perturbative and/or Markovian limits. If one effect is to interact strongly with another effect, by contrast, then the time/energy scales of the two effects should be similar. As we have shown here, the maximum efficiency of quantum transport is attained when the key decoherence parameter $k_B\lambda T/\hbar\gamma$ is on the same order as the free Hamiltonian coherent time-scale $g$. As shown in Refs. 32, 34, 36, and 65 environmentally assisted quantum transport is an important effect. This *convergence* of time scales is a nuisance for quantum simulation, as perturbative methods break down. While this phenomenon makes the efficient simulation of such systems very difficult, the convergence of time scales is quite useful for nature, however, as the two effects can now interact strongly with each other to produce a significant enhancement in efficiency. Of course, too strong interaction could also produce a significant decrease in efficiency. But for systems undergoing natural selection, one typically expect that the strong interaction is tuned at the right level to give rise to a beneficial effect.

The results of this paper illustrate the quantum Goldilocks principle manifestation in the FMO complex and other small-size multichromophoric configurations: the time/energy scales have converged within the range where the different quantum effects and structural parameters at work can interact strongly with each other to give rise to possibility of high efficient energy transport. Moreover, this variety of quantum effects can be combined to attain high efficiency without sacrificing robustness. The convergence of time scales makes these complexes difficult to model, but highly efficient in certain instances. We anticipate that a similar convergence of time/energy scales could appear in larger biomolecular complexes, nanostructures, and in biological processes where quantum mechanics might play an important role.

The possibility of a quantum Goldilocks principle opens many new doors for further investigations. In particular, it will be of significant importance to explore underlying physical explanations for the existence of quantum Goldilocks principle, the possible fundamental mechanisms, and environmental conditions under which this phenomenon becomes relevant for disorder and noisy complex quantum systems, and the general classes of physical and engineering problems that could be optimized by this guiding principle.

## ACKNOWLEDGMENTS

We thank A. Aspuru-Guzik, A. Ishizaki, M. Sarovar, K. B. Whaley, for useful discussions. We also thank J. H. Choi and D. Hayes for helping us with extracting the FMO data. We acknowledge funding from DARPA under the QuBE program (M.M., A.S., S.L., H.R.), ENI (M.M., S.L.), NSERC and Google (M.M.) and NSF (S.L., A.S., H.R.), and ISI, NEC, Lockheed Martin, Intel (S.L.).

TABLE II. Spatial location of Bchls and their dipole moment orientation.

| Bchl | x (Å) | y (Å) | z (Å) | $\theta$ | $\phi$ |
|---|---|---|---|---|---|
| 1 | 28.032 | 163.534 | 94.400 | 0.3816 | $-0.6423+\pi$ |
| 2 | 17.140 | 168.057 | 100.162 | 0.067 | $0.5209+\pi$ |
| 3 | 5.409 | 180.553 | 97.621 | 0.1399 | $1.3616+\pi$ |
| 4 | 9.062 | 187.635 | 89.474 | 0.257 | $-0.6098+\pi$ |
| 5 | 21.823 | 185.260 | 84.721 | $-0.1606$ | $0.6899+\pi$ |
| 6 | 23.815 | 173.888 | 82.810 | $-0.4214$ | $-1.4686+\pi$ |
| 7 | 12.735 | 174.887 | 89.044 | 0.578 | $-1.0076+\pi$ |

## APPENDIX A: FMO FREE HAMILTONIAN

In this work we use the following free Hamiltonian for the FMO complex, given in Ref. 7:

$$H = \begin{pmatrix} 280 & -106 & 8 & -5 & 6 & -8 & -4 \\ -106 & 420 & 28 & 6 & 2 & 13 & 1 \\ 8 & 28 & 0 & -62 & -1 & -9 & 17 \\ -5 & 6 & -62 & 175 & -70 & -19 & -57 \\ 6 & 2 & -1 & -70 & 320 & 40 & -2 \\ -8 & 13 & -9 & -19 & 40 & 360 & 32 \\ -4 & 1 & 17 & -57 & -2 & 32 & 260 \end{pmatrix}.$$

The estimated values of dipole moment orientations and positions of the Mg atoms, representing the location of Bchls, are extracted from the pdb file of the FMO complex.[84] These data can be summarized in Table II.

The Bchl-Bchl coupling in FMO is dipole-dipole interaction

$$J_{jk} = \frac{C}{R_{jk}^3}\left(\mu_j \cdot \mu_k - \frac{3}{R_{jk}^2}(\mu_j \cdot \mathbf{R}_{jk})(\mu_k \cdot \mathbf{R}_{jk})\right), \quad \text{(A1)}$$

for which we choose the constant $C|\mu|^2 = 134\,000$ cm$^{-1}$ Å$^3$.[18]

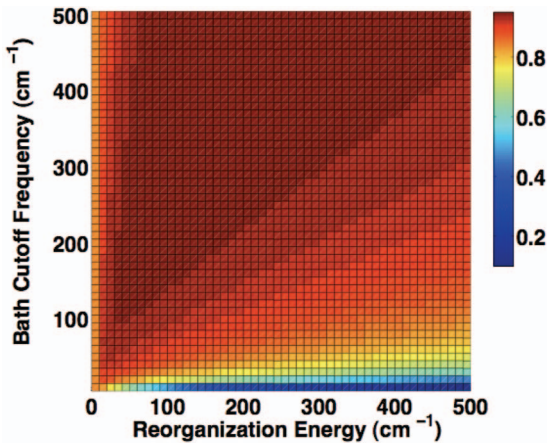


FIG. 8. The top view of FMO energy transfer landscape in the presence of an Ohmic model of bath spectral density as a function of reorganization energy and bath frequency cutoff at room temperature. The ETE predicted by this model is below the estimate values by a Lorentzian model and therefore it cannot explain near ideal performance of FMO complex in exciton transport. Nevertheless, here we can also observe the three distinct regimes of weak and strong localizations close to $\gamma$ and $\lambda$ axes, and the intermediate optimal ENAQT, separated by straight lines. This plot confirms the role of parameter $k_B\lambda T/\hbar\gamma$ as an effective governing parameter.

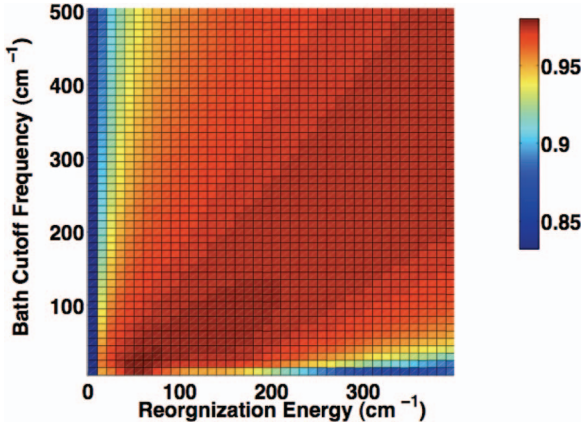


FIG. 9. Top view of the ETE landscape at 77 K for a bath with a Lorentzian spectral density. The general pattern of an optimal transport region in between two limits of localized low-efficient transport regimes, divided by rather straight lines, is observed here as well. However, due to low-temperature effects captured in the parameter $k_B\lambda T/\hbar\gamma$, the adversarial high reorganization and slow bath effects become less pronounced leading to a higher ETE than those in Fig. 3 in the corresponding limits.

## APPENDIX B: ENERGY TRANSFER EFFICIENCY FOR OHMIC BATH AND CRYOGENIC TEMPERATURE

Here, we demonstrate that separation of ETE landscape, as a function of the parameter $k_B\lambda T/\hbar\gamma$, into the various regions with distinct quantum transport efficiencies is not a mere property of either Lorentzian bath or high temperature limit. A top view of FMO energy transfer landscape is shown for an Ohmic spectral density at 298 K and Lorentzian spectral density at 77 K in Figs. 8 and 9, respectively. In each figure, one can distinguish three different regions including low-efficient weakly localized limit, optimal EANQT, and low-efficient strongly localized limit, similar to the results presented in Fig. 3.

It should be noted that a bath with an Ohmic regularized spectral density, $J(\omega) = \lambda(\omega/\gamma)\exp(-\omega/\gamma)$, has often been employed in modeling the effect of bath fluctuations on the spectroscopic readout of an FMO sample.[7,71] Figure 8 presents the top view of ETE landscape as a function of bath reorganization energy and cutoff frequency with an Ohmic density. The observed high efficient region stays lower than its Lorentzian counterpart in Fig. 3, therefore is unable to explain the high efficiency of the FMO complex. This can be seen as a confirmation for the theoretical modeling of the solvent-protein environment with Lorentzian spectral densities.[57]

[1] R. E. Blankenship, *Molecular Mechanism of Photosynthesis* (Blackwell Science, London, 2002).
[2] R. K. Chain and D. I. Arnon, Proc. Natl. Acad. Sci. U.S.A. **74**, 3377 (1977).
[3] *Quantum Effects in Biology*, edited by M. Mohseni, Y. Omar, G. Engel, and M. Plenio (Cambridge University Press, Cambridge, UK, 2014).
[4] V. Chernyak and S. Mukamel, J. Chem. Phys. **105**, 4565 (1996).
[5] W. M. Zhang, T. Meier, V. Chernyak, and S. Mukamel, J. Chem. Phys. **108**, 7763 (1998).
[6] V. I. Novoderezhkin, M. A. Palacios, H. van Amerongen, and R. van Grondelle, J. Phys. Chem. B **108**, 10363 (2004).
[7] M. Cho, H. M. Vaswani, T. Brixner, J. Stenger, and G. R. Fleming, J. Phys. Chem. B **109**, 10542 (2005).
[8] M. Grover and R. Silbey, J. Chem. Phys. **54**, 4843 (1971).
[9] H. Haken and G. Strobl, Z. Phys. **262**, 135 (1973).

[10]V. M. Kenkre and P. Reineker, *Exciton Dynamics in Molecular Crystals and Aggregates* (Springer, Berlin, 1982).
[11]X. Hu, T. Ritz, A. Damjanović, and K. J. Schulten, Phys. Chem. B **101**, 3854 (1997).
[12]T. Ritz, S. Park, and K. Schulten, J. Phys. Chem. B **105**, 8259 (2001).
[13]G. D. Scholes and G. R. Fleming, J. Phys. Chem. B **104**, 1854 (2000).
[14]G. D. Scholes, X. J. Jordanides, and G. R. Fleming, J. Phys. Chem. B **105**, 1640 (2001).
[15]M. Yang and G. R. Fleming, Chem. Phys. **275**, 355 (2002).
[16]V. May and O. Kuhn, *Charge and Energy Transfer Dynamics in Molecular Systems* (Wiley-VCH, Weinheim, 2004).
[17]S. Jang, M. D. Newton, and R. J. Silbey, Phys. Rev. Lett. **92**, 218301 (2004).
[18]J. Adolphs and T. Renger, Biophys. J. **91**, 2778 (2006).
[19]G. S. Engel, T. R. Calhoun, E. L. Read, T. K. Ahn, T. Mancal, Y. C. Cheng, R. E. Blankenship, and G. R. Fleming, Nature (London) **446**, 782 (2007).
[20]A. Shabani, M. Mohseni, H. Rabitz, and S. Lloyd, Phys. Rev. E **86**, 011915 (2012).
[21]T. Förster, in *Modern Quantum Chemistry, Istanbul Lectures*, edited by O. Sinanoglu (Academic, New York, 1965), Vol. 3, pp. 93–137.
[22]G. D. Scholes, Annu. Rev. Phys. Chem. **54**, 57–87 (2003).
[23]A. G. Redfield, Adv. Magn. Reson. **1**, 1 (1965).
[24]H. Lee, Y.-C. Cheng, and G. R. Fleming, Science **316**, 1462 (2007).
[25]T. R. Calhoun, N. S. Ginsberg, G. S. Schlau-Cohen, Y.-C. Cheng, M. Ballottari, R. Bassi, and G. R. Fleming, J. Phys. Chem. B **113**, 16291 (2009).
[26]I. Mercer, Y. El-Taha, N. Kajumba, J. Marangos, J. Tisch, M. Gabrielsen, R. Cogdell, E. Springate, and E. Turcu, Phys. Rev. Lett. **102**, 057402 (2009).
[27]E. Collini and G. D. Scholes, Science **323**, 369 (2009).
[28]E. Collini, C. Y. Wong, K. E. Wilk, P. M. Curmi, P. Brumer, and G. D. Scholes, Nature (London) **463**, 644 (2010).
[29]G. Panitchayangkoon, D. Hayes, K. A. Fransted, J. R. Caram, E. Harel, J. Wen, R. E. Blankenship, and G. S. Engel, Proc. Nat. Acad. Sci. U.S.A. **107**, 12766 (2010).
[30]A. F. Fidler, J. R. Caram, D. Hayes, and G. S. Engel, J. Phys. B **45**, 154013 (2012).
[31]D. Hayes and G. S. Engel, Phil. Trans. R. Soc. A **370**, 3692 (2012).
[32]M. Mohseni, P. Rebentrost, S. Lloyd, and A. Aspuru-Guzik, J. Chem. Phys. **129**, 174106 (2008).
[33]P. Rebentrost, M. Mohseni, and A. Aspuru-Guzik, J. Phys. Chem. B **113**, 9942 (2009).
[34]P. Rebentrost, M. Mohseni, I. Kassal, S. Lloyd, and A. Aspuru-Guzik, New J. Phys. **11**, 033003 (2009).
[35]M. B. Plenio and S. F. Huelga, New J. Phys. **10**, 113019 (2008).
[36]F. Caruso, A. W. Chin, A. Datta, S. F. Huelga, and M. B. Plenio, J. Chem. Phys. **131**, 105106 (2009).
[37]A. Olaya-Castro, C. F. Lee, F. Fassioli Olsen, and N. F. Johnson, Phys. Rev. B **78**, 085115 (2008).
[38]A. Ishizaki and G. R. Fleming, J. Chem. Phys. **130**, 234110 (2009).
[39]A. Ishizaki and G. R. Fleming, J. Chem. Phys. **130**, 234111 (2009).
[40]A. Ishizaki and G. R. Fleming, Proc. Nat. Acad. Sci. U.S.A. **106**, 17255 (2009).
[41]J. Cao and R. Silbey, J. Phys. Chem. A **113**, 13826 (2009).
[42]S. Hoyer, M. Sarovar, and K. B. Whaley, New J. Phys. **12**, 065041 (2010).
[43]F. Caruso, A. W. Chin, A. Datta, S. F. Huelga, and M. B. Plenio, Phys. Rev. A **81**, 062346 (2010).
[44]M. Sarovar, A. Ishizaki, G. R. Fleming, and K. B. Whaley, Nat. Phys. **6**, 462 (2010).
[45]J. Yuen-Zhou, J. Krich, M. Mohseni, and A. Aspuru-Guzik, Nat. Acad. Sci. U.S.A. **108**, 17615 (2011).
[46]S. Lloyd and M. Mohseni, New J. Phys. **12**, 075020 (2010).
[47]D. Abasto, M. Mohseni, S. Lloyd, and P. Zanardi, Philos. Trans. R. Soc. London, Ser. A **3750**, 37013 (2012).
[48]H.-P. Breuer and F. Petruccione, *The Theory of Open Quantum Systems* (Oxford University Press, New York, 2002).
[49]R. Kubo, Adv. Chem. Phys. **15**, 101 (1969), Y. Tanimura and R. Kubo, J. Phys. Soc. Jpn. **58**, 101 (1989).
[50]J. Cao, J. Chem. Phys. **107**, 3204 (1997).
[51]S. Jang, Y. Cheng, D. R. Reichman, and J. D. Eaves, J. Chem. Phys. **129**, 101104 (2008).
[52]Q. Shi, L. Chen, G. Nan, R. X. Xu, and Y. J. Yan, J. Chem. Phys. **130**, 084105 (2009).
[53]A. Nazir, Phys. Rev. Lett. **103**, 146404 (2009).
[54]J. Prior, A. W. Chin, S. F. Huelga, and M. B. Plenio, Phys. Rev. Lett. **105**, 050404 (2010).
[55]X. T. Liang, Phys. Rev. E **82**, 051918 (2010); I. de Vega, preprint arXiv:1005.0465 (2010).
[56]H. Fujisaki, Y. Zhang, and J. E. Straub, preprint arXiv:1003.4796 (2010).
[57]J. Gilmore and R. H. McKenzie, J. Phys. Chem. A **112**, 2162 (2008).
[58]E. L. Read, G. S. Schlau-Cohen, G. S. Engel, J. Wen, R. E. Blankenship, and G. R. Fleming, Biophys. J. **95**, 847 (2008).
[59]Y.-Z. Ma, R. A. Miller, G. R. Fleming, and M. B. Francis, J. Phys. Chem. B **112**, 22 (2008).
[60]R. A. Miller, N. Stephanopoulos, J. M. McFarland, A. S. Rosko, P. L. Geissler, and M. B. Francis, J. Am. Chem. Soc. **132**, 6068–6074 (2010).
[61]R. E. Fenna and B. W. Matthews, Nature (London) **258**, 573 (1975); B. W. Matthews, R. E. Fenna, M. C. Bolognesi, M. F. Schmid, and J. M. Olson, J. Mol. Biol. **131**, 259 (1979).
[62]Y. F. Li, W. Zhou, R. E. Blankenship, and J. P. Allen, J. Mol. Biol. **271**, 456471 (1997).
[63]H.-P. Breuer, E. M. Laine, and J. Piilo, Phys. Rev. Lett. **103**, 210401 (2009).
[64]P. Rebentrost and A. Aspuru-Guzik, preprint arXiv:1011.3809 (2010).
[65]J. Wu, F. Liu, Y. Shen, J. Cao, and R. J. Silbey, e-print arXiv:1008.2236.
[66]M. Mohseni, A. Shabani, S. Lloyd, Y. Omar, and H. Rabitz, J. Chem. Phys. **138**, 204309 (2013).
[67]B. Krameri and A. MacKinnont, Rep. Prog. Phys. **56**, 1469 (1993).
[68]P. Reineker and K. Kassner, J. Lumin. **40–41**, 467 (1988).
[69]P. Castiglione, J. Phys. A: Math. Gen. **33**, 1975 (2000).
[70]I. Goychuk and P. Hänggi, Adv. Phys. **54**, 525 (2005).
[71]G. R. Fleming and M. H. Cho, Annu. Rev. Phys. Chem. **47**, 109 (1996).
[72]F. Fassioli, A. Nazir, and A. Olaya-Castro, J. Phys. Chem. Lett. **1**, 2139 (2010).
[73]M. Sarovar, Y. Cheng, and K. B. Whaley, Phys. Rev. E **83**, 011906 (2011).
[74]A. Ishizaki, T. R. Calhoun, G. S. Schlau-Cohen, and G. R. Fleming, Phys. Chem. Chem. Phys. **12**, 7319 (2010).
[75]N. Demirdöven, M. Khalil, and A. Tokmakoff, Phys. Rev. Lett. **89**, 237401 (2002); M. Khalil, N. Demirdöven, and A. Tokmakoff, J. Phys. Chem. A **107**, 5258 (2003).
[76]C. Olbrich, J. Strümpfer, K. Schulten, and U. Kleinekathöfer, J. Phys. Chem. B **115**, 758 (2011).
[77]D. A. Lidar, I. L. Chuang, and K. B. Whaley, Phys. Rev. Lett. **81**, 2594 (1998); M. Mohseni, J. S. Lundeen, K. J. Resch, and A. M. Steinberg, *ibid.* **91**, 187903 (2003); A. Shabani and D. A. Lidar, Phys. Rev. A **72**, 042303 (2005).
[78]A. W. Chin, J. Prior, R. Rosenbach, F. Caycedo-Soler, S. F. Huelga, and M. B. Plenio, Nat. Phys. **9**, 113 (2013); V. Tiwari, W. K. Peters, and D. M. Jonas, Proc. Natl. Acad. Sci. U.S.A. **110** (4) 1203 (2013); E. J. O'Reilly and A. Olaya-Castro, e-print arXiv:1301.6970.
[79]S. Lloyd, Lecture at Santa Fe Institute, 1990, as reported by M. Gell-Mann, The Quark and the Jaguar.
[80]R. J. Huggett, *Geoecology: An Evolutionary Approach* (Routledge, London, 1995).
[81]T. Hulubei, E. C. Freuder, and R. J. Wallace, Artif. Intell. Eng. Des., Anal. Manuf. **17**, 3 (2013).
[82]C. P. Canlas, J. Lu, N. A. Ray, N. A. Grosso-Giordano, S. Lee, J. W. Elam, R. E. Winans, R. P. Van Duyne, P. C. Stair, and J. M. Notestein, Nat. Chem. **4**, 1030 (2012).
[83]S. J. Martin, Autophagy **7**, 922 (2011).
[84]The FMO PDB file was provided by M. Cho laboratory.
[85]A. Shabani, M. Mohseni, H. Rabitz, and S. Lloyd, "Numerical evidence for robustness of environment-assisted quantum transport" (unpublished).